

# Renormalized charge in a two-dimensional model of colloidal suspension from hypernetted chain approach

Manuel Camargo and Gabriel Téllez\*  
Departamento de Física  
Universidad de los Andes  
A.A. 4976, Bogotá, Colombia.

## Abstract

The renormalized charge of a simple two-dimensional model of colloidal suspension was determined by solving the hypernetted chain approximation and Ornstein-Zernike equations. At the infinite dilution limit, the asymptotic behavior of the correlations functions is used to define the effective interactions between the components of the system and these effective interactions were compared to those derived from the Poisson-Boltzmann theory. The results we obtained show that, in contrast to the mean-field theory, the renormalized charge does not saturate, but exhibits a maximum value and then decays monotonically as the bare charge increases. The results also suggest that beyond the counterion layer near to the macroion surface, the ionic cloud is not a diffuse layer which can be handled by means of the linearized theory, as the two-state model claims, but a more complex structure is settled by the correlations between microions.

PACS: 82.70.Dd, 61.20.Gy, 61.20.Qg

## 1 Introduction

The omnipresence of colloidal suspensions in chemistry and biology, and the variety and tunability of their particle interactions explains their importance both in industrial applications and fundamental research. A complete statistical

---

\*gtellez@uniandes.edu.co

description of this kind of systems is an extremely complex task inasmuch as that description must include the interaction between all of the species constituting the system: colloids, suspended ions and molecules of the solvent. However, as a result of the high asymmetry of mass and charge, one hopes that a suitable approach is obtained by considering the system, not as a mixture, but as a “new” monodispersed system which involves only colloidal particles (macroions) interacting through an effective potential [1, 2].

In the framework of the approaches based on linearized Poisson-Boltzmann theory, it is found that the effective interaction between two macro-ions exhibits a Debye-Hückel-like (DH) behavior due to the screening effect produced by ions present in the surrounding medium. As the charge of macroions ( $Q$ ) increases, the linear approximation becomes inadequate and it is necessary to use other approaches. Nevertheless, these approaches show that at large distances the effective interaction continues to have a DH-like behavior but it is necessary to replace the charge  $Q$  by an effective or renormalized charge  $Q_{ren}$ . Then, the concept of charge renormalization simplifies the description of colloidal interactions and gives us some insights about the phase behavior of the colloidal suspensions. However, it remains problematic to find methods that allow their evaluation for arbitrary conditions of charge and concentration.

In this work we evaluate the renormalized charge for a two-dimensional (2D) Coulomb system. For this purpose, we solve numerically the Ornstein-Zernike (OZ) equation in the scope of the hypernetted chain (HNC) approximation and we use the calculated potential of mean force as the effective interaction between the components of the system. The renormalized charge, numerically evaluated, is then compared to the one predicted by theoretical models based on the Poisson-Boltzmann (PB) theory. The results obtained show that, in contrast to the mean-field theory, the renormalized charge does not saturate, but exhibits a maximum value and then decays monotonically as the bare charge increases. The results also suggest that beyond the counterion layer near to the macroion surface, the ionic cloud is not a diffuse layer which can be handled by means of the linearized theory, as the two-state model claims, but a more complex structure is settled by the correlations between microions.

We use a two-dimensional system due to two main reasons. In the first place, classical two-dimensional Coulomb systems with logarithmically interacting particles are simplified models which keep the Coulomb nature of the particle interaction. Besides, by using field theoretical tools, some of these models admit an exact solution, which makes it possible to judge the quality of approximate formulations. On the other hand, 2D Coulomb systems can be used to model stiff rod-like polyelectrolytes, which interact with the ions present in the solvent via a logarithmic potential.

This article is organized as follows. In section 2 we describe briefly the system considered. Section 3 is devoted to explain the numerical method used to solve

the OZ and HNC equations. The central part of this work is presented in section 4, where the numerical results of the HNC calculations are displayed and discussed for two models of 2D Coulomb systems: the guest particle system and a simple model of colloidal suspensions at the infinite dilution limit. Finally, some conclusions are summarized in the last section.

## 2 Guest charge in an electrolyte

In order to take the first steps toward a solution of the renormalized charge problem in colloidal suspensions at the infinite dilution limit, we consider the properties of a “guest” charge immersed in an electrolyte, which is modeled as a two-dimensional two-component plasma (2D-TCP). We consider here a system composed by a single central guest particle with charge  $Q = Ze$  and radius  $\sigma_0$  immersed in a 2D-TCP formed by negatively and positively hard-disks ions of radius  $\sigma_{\pm} = \sigma$  and charges  $q_{\pm} = \pm z_{\pm}e$  (with  $z_{\pm} > 0$ ). The bulk densities of positive and negative ions are denoted by  $n_+$  and  $n_-$ , and the total density is  $n = n_+ + n_-$ . The electrolyte is globally neutral,  $q_+n_+ + q_-n_- = 0$ . The interaction potential between disks  $i$  and  $j$ , separated by a distance  $r_{ij}$ , is given by

$$\beta u_{ij}(r_{ij}) = \begin{cases} \infty & r_{ij} < \sigma_i + \sigma_j \\ \beta v_{ij}(r_{ij}) = -z_i z_j \text{sign}(q_i q_j) \Gamma \ln\left(\frac{r_{ij}}{L}\right) & r_{ij} > \sigma_i + \sigma_j \end{cases} \quad (1)$$

where  $\beta$ ,  $z_i$ , and  $\Gamma = \beta e^2$  are, respectively, the inverse temperature, the valence of the charge  $i$  and the coupling (strength) parameter.  $L$  is an irrelevant length scale used to fix the zero of the Coulomb potential. At the limit of point-like charges,  $\sigma_0 = 0$  and  $\sigma = 0$ , the system is stable against the collapse of positive and negative particles provided  $-2/z_+ < Z\Gamma < 2/z_-$  and  $z_+ z_- \Gamma < 2$ .

From field theoretical arguments in the limit  $\sigma_0 \rightarrow 0$  and  $\sigma = 0$ , the asymptotic large-distance behavior of the effective interaction between the guest particle and the TCP charges is related to the large-distance behavior of the corresponding two-points correlation function of the exponential fields associated to the 2D sine-Gordon theory [3, 4]. According to this correspondence, the asymptotic behavior of the effective interaction can be exactly evaluated and this result indicates that the electrostatic potential produced by the guest charge has the same asymptotic behavior as the one evaluated through the DH approach provided that both the inverse decay length and the charge are adequately renormalized.

On the other hand, the short-distance asymptotics of the density profiles of the coions and counterions near the guest charge has been studied for the symmetric case, i.e.  $z_{\pm} = 1$  [5, 6]. In this case, it has been shown that the coion density profile exhibit a change of behavior if the guest charge becomes large enough ( $Z\Gamma \geq 2 - \Gamma$ ). This behavior has been interpreted as a first step of the counterion

condensation (for large coulombic coupling); the second step taking place at the usual Manning-Oosawa threshold ( $Z\Gamma = 2$ ).

Naturally, the latter effect is related to the settlement of the renormalized charge. In this way, it can be stated that this model encloses the most important facts involved in the non-linear screening phenomenon. In order to compare these exact results with the numerical ones in more general conditions, we have calculated the correlation functions between the different components of the system by solving the OZ and HNC equations as described below.

### 3 Numerical method

As usual, we denote by  $g_{ij}(r)$ ,  $h_{ij}(r) = g_{ij}(r) - 1$  and  $c_{ij}(r)$  the radial distribution function, the total correlation function and the direct correlation function, respectively, between two components  $i$  and  $j$  of the system separated by a distance  $r$ . The subscripts  $i$  and  $j$  can be  $+$ ,  $-$ , or  $0$ , denoting respectively a positive ion, a negative ion, or the guest charge. The OZ equations for a multicomponent system reads

$$h_{ij}(|\mathbf{r}_1 - \mathbf{r}_2|) = c_{ij}(|\mathbf{r}_1 - \mathbf{r}_2|) + \sum_k n_k \int h_{ik}(|\mathbf{r}_1 - \mathbf{r}_3|) c_{kj}(|\mathbf{r}_3 - \mathbf{r}_2|) d\mathbf{r}_3 \quad (2)$$

where  $n_k$  the density of the species  $k$ . In the infinite dilution limit considered here,  $n_0 = 0$ , the OZ equations describing the correlation functions between ions of the TCP do not involve the guest charge. By defining  $\gamma_{ij}(r) = h_{ij}(r) - c_{ij}(r)$ , these equations can be written in the Fourier space as

$$\hat{\gamma}_{++}(k) = \frac{(1 - D(k)) \hat{c}_{++}(k) + n_- (\hat{c}_{+-}^2(k) - \hat{c}_{++}(k) \hat{c}_{--}(k))}{D(k)} \quad (3)$$

$$\hat{\gamma}_{+-}(k) = \frac{\hat{c}_{+-}(k)(1 - D(k))}{D(k)} \quad (4)$$

$$\hat{\gamma}_{--}(k) = \frac{(1 - D(k)) \hat{c}_{--}(k) + n_+ (\hat{c}_{+-}^2(k) - \hat{c}_{++}(k) \hat{c}_{--}(k))}{D(k)} \quad (5)$$

where the hat denotes the Fourier transform of a function, and  $D(k) = (1 - n_+ \hat{c}_{++}(k))(1 - n_- \hat{c}_{--}(k)) - n_+ n_- \hat{c}_{+-}^2(k)$ . The guest charge-ion correlation functions, in the infinite dilution limit, satisfy

$$\hat{\gamma}_{0+}(k) = \frac{\hat{c}_{0+}(k) (1 - n_- \hat{c}_{--}(k) - D(k)) + n_- \hat{c}_{0-}(k) \hat{c}_{+-}(k)}{D(k)} \quad (6)$$

$$\hat{\gamma}_{0-}(k) = \frac{\hat{c}_{0-}(k) (1 - n_+ \hat{c}_{++}(k) - D(k)) + n_+ \hat{c}_{0+}(k) \hat{c}_{+-}(k)}{D(k)}. \quad (7)$$

In order to solve equations (3)–(7) it is necessary to split functions  $\gamma(r)$  and  $c(r)$  in short- and large-distance components. Since  $h(r) \rightarrow 0$  y  $c(r) \rightarrow -\beta v(r)$

when  $r \rightarrow \infty$ , it may be written

$$v(r) = v^{(s)}(r) + v^{(l)}(r), \quad c(r) = c^{(s)}(r) - \beta v^{(l)}(r), \quad \gamma(r) = \gamma^{(s)}(r) + \beta v^{(l)}(r)$$

where the large-distance component of the potential is chosen to be  $v^{(l)}(r) = (1 - e^{-\alpha r})v(r)$  with  $\alpha$  a cutoff parameter. In this way, the corresponding HNC closure relations are defined through

$$g_{ij}(r) = \begin{cases} 0 & r < \sigma_i + \sigma_j \\ \exp\left(\gamma_{ij}^{(s)}(r) - \beta v_{ij}^{(s)}(r)\right) & r \geq \sigma_i + \sigma_j \end{cases}$$

$$c_{ij}^{(s)}(r) = g_{ij}(r) - 1 - \gamma_{ij}^{(s)}(r) \quad (8)$$

with  $v_{ij}^{(s)}(r)$  the short-range part of the Coulomb potential.

Equations (3)–(8) were solved by using a direct iterative method. In order to improve convergence, the new input function for iteration  $i + 1$ ,  $c_{\text{in}}^{(i+1)}(r)$ , was evaluated by using a linear relaxation (Broyles' mixing of the old input function  $c_{\text{in}}^{(i)}(r)$  and the output function  $c_{\text{out}}^{(i)}(r)$ )

$$c_{\text{in}}^{(i+1)}(r) = c_{\text{in}}^{(i)}(r) + \mu \left( c_{\text{out}}^{(i)}(r) - c_{\text{in}}^{(i)}(r) \right) \quad (9)$$

where  $\mu$  ( $0 \leq \mu \leq 1$ ) is the relaxation parameter. The numerical evaluation of the two-dimensional Fourier transform was carried out through the quasi-discrete Hankel transform method [7], by using  $N = 6000$  grid points and maximum radius  $10 < \kappa R < 16$ , with  $\kappa$  the inverse Debye length ( $\kappa^2 = 2\pi z_+ z_- n \Gamma$ ). The iterations were stopped when the larger difference between successive  $c(r)$ 's was less than  $10^{-6}$ , i.e.

$$\tau = \max |c_{\text{out}}^{(i+1)}(r) - c_{\text{out}}^{(i)}(r)| \leq 10^{-6}. \quad (10)$$

Finally, the numerical accuracy was monitored by checking both the electroneutrality condition and the Stillinger-Lovett screening sum rule [8]. In all the considered cases, the numeric results for these conditions differ at most by 0.01% with regard to the theoretical values.

## 4 Results

In order to calculate the renormalized charge  $Z_{ren}$  we follow a similar procedure to the described one in [9]. Let us recall that under the DH approximation the potential of mean force  $w_{0s}^{\text{DH}}(r)$  between the guest charge and an ion of type  $s = \pm$  is given by

$$-\beta w_{0s}^{\text{DH}}(r) = \frac{\Gamma Z z_s}{\kappa \sigma_c K_1(\kappa \sigma_c)} K_0(\kappa r) \quad (11)$$

with  $K_0$  and  $K_1$  the modified Bessel functions of order 0 and 1, and  $\sigma_c = \sigma_0 + \sigma$ .

Once the correlation functions  $g_{0\pm}(r)$  are iteratively evaluated from the OZ equations, the potential of mean force  $w_{0\pm}(r)$  is obtained from the definition  $g_{0\pm}(r) = e^{-\beta w_{0\pm}(r)}$ . We assume that, at large distances  $\kappa r \gg 1$ , the potential of mean force has a DH-like functional form, i.e.  $w(r) \propto K_0(\kappa_{ren}r) \sim \sqrt{\pi} \exp(-\kappa_{ren}r) / \sqrt{(2\kappa_{ren}r)}$ . Besides, we can also assume that all correlation functions fall off in the same way at large distances. These assumptions are supported in the exact solution for point-like particles, which indicates that in the stability region the correlation functions exhibit a DH behavior. However, it is necessary to renormalize not only the charge  $Z_{ren}$  but also the decay length  $\kappa_{ren}^{-1}$  [3].

In this way, we may suppose that

$$-\beta w_{0s}(r) = \ln g_{0s}(r) \sim A_{0s} \frac{\exp(-\kappa_{ren}r)}{\sqrt{r}} \quad (12)$$

where

$$A_{0s} = \sqrt{\frac{\pi}{2\kappa_{ren}}} \frac{\Gamma Z_{ren} z_s}{\kappa_{ren} \sigma_c K_1(\kappa_{ren} \sigma_c)}. \quad (13)$$

Then, the parameters  $A_{0s}$  and  $\kappa_{ren}$  can be obtained from a linear fit of the functions

$$L_{0s}(r) = \ln(\sqrt{r} |\ln g_{0s}(r)|) = \ln(|A_{0s}|) - \kappa_{ren}r \quad (14)$$

for  $r$  values large enough. We select the range of  $r$  to be used in the fit through the condition  $10^{-4} \leq |\log g_{0s}(r)| \leq 10^{-2}$ . We choose this range because the values of the fitted functions are two orders of magnitude greater than the tolerance and the numerical uncertainties (see eq. (10)). In some cases, the correlation functions exhibit an oscillation and then it also becomes necessary to impose empirically a minimum value for  $\kappa r$ .

## 4.1 Guest charge

### 4.1.1 Symmetric TCP

We consider all particles as equally sized hard-disks satisfying  $\kappa \sigma_0 = \kappa \sigma = 10^{-2}$ , and the ions have charges  $z_{\pm} = 1$ . In figure 1 are shown the correlation functions between the guest charge and the ions of a symmetric TCP for different values of  $Z > 0$  and the coupling parameter  $\Gamma$ . Qualitatively, these profiles are consistent with the common image of an ionic cloud (mainly formed by counterions) surrounding the central charge. From the figure, it is clear that for  $\Gamma = 0.2$  the correlation functions  $g_{0\pm}(r)$  behave monotonically for all displayed values of  $Z\Gamma$ . However, when  $\Gamma = 0.4$  and  $Z\Gamma = 3$  the correlation function  $g_{0+}(r)$  exhibit a peak at  $\kappa r \approx 0.1$ , which rise up as a consequence of the increase

of  $g_{0-}$  jointly with more marked microions correlations, as it can be seen in figure 2.

As stated before, the renormalized parameters were evaluated from a linear fit (in a least squares sense) of the functions  $L_{0\pm}(r)$  similar to the ones shown in figure 3, whose non-linear behavior extends roughly from  $\kappa r = 0$  to  $\kappa r \approx 1$ . From now on, a computed renormalized parameter is equivalent to the mean value of the two ones obtained from both  $L_{0+}(r)$  and  $L_{0-}(r)$  taken independently. Note that the curves were calculated at  $Z\Gamma = 3$  which correspond to strong coupling regime between the guest charge and the microions.

We explored a range of couplings  $0.1 \leq \Gamma \leq 0.5$ . Within this range, the renormalized inverse screening length  $\kappa_{ren}$  is found to be systematically smaller than  $\kappa$ , and it is a decreasing function of the coupling  $\Gamma$ , in agreement with the exact results [3]. However  $\kappa_{ren}/\kappa$  only differs from 1 by at most 2% for the largest coupling  $\Gamma = 0.5$ .

Figure 4 displays  $Z_{ren}$  at different coupling parameters. In contrast to the PB prescription,  $Z_{ren}$  is not a monotonically increasing function of  $Z$ , but it displays a maximal value after which it drops to a point where the implemented iterative method fails to converge. This behavior qualitatively resembles the one predicted by the exact solution when the microions and the guest charge are considered as point-like particles ( $\sigma = 0$ ) and a small hard disk ( $\kappa\sigma_0 \rightarrow 0$ ), respectively. According to this result, the renormalized charge exhibit a maximum at  $Z_m\Gamma = 2 - \Gamma/2$  and decrease until the collapse point  $Z_c\Gamma = 2$  at which  $Z_{ren} = Z_c - 1$ , as indicated by the dotted line in figure 4. This behavior reflects the effect of the counterion condensation, i.e. the renormalized charge associated with the collapse value  $Z_c$  of the bare charge is identical to that of the bare charge  $Z_c - 1$  because of the condensation of one counterion from the TCP onto the guest particle [3, 4]. By increasing  $Z$  further more counterions become condensed and the previous description predicts a renormalized charge oscillating between two extremes.

As it can be noted from figure 4, as  $\Gamma$  decreases,  $Z_{ren}$  moves closer to the mean-field PB theory predicted values; however, the renormalized charge predicted by PB theory is always greater than the one computed from HNC approach. Naturally, this behavior can be ascribed to the correlations between the components of the system and in a minor grade, to the finite radius of the ions, as it will become clearer below. When the coupling becomes stronger, the HNC collapse point is closer to the one predicted for point-like particles, i.e.  $Z\Gamma = 2$ . Although, in the other cases the hard-disk potential inclusion allows us to go beyond this point, at  $\Gamma = 0.5$  we found that the coupling between the guest particle and the counterions is strong enough to provoke the divergence of the HNC method at smaller values of  $Z\Gamma$ . This effect can be related to the short-range structure of the correlations between the guest particle and the microions.

By using the sine-Gordon model for the TCP, it has been argued that a change in the short-range behavior of the coion density profile can be interpreted as a “precursor” of the (Manning) counterion condensation [5]. When  $Z\Gamma$  increases above  $2 - \Gamma$  ( $Z\Gamma < 2$ ,  $\Gamma < 2$ ), the coion cloud  $n_+(r) = n_+g_{0+}(r)$  shows a change of behavior near the guest particle. This fact is reflected in the parameter  $\alpha_{0\pm}$  describing the potential of mean force for short-distances defined below. Near the guest charge this latter must correspond to the Coulomb potential, i.e.

$$-\beta w_{0s}(r) = \ln g_{0s}(r) \underset{r \rightarrow \sigma_0}{\sim} \alpha_{0s} \ln r \quad (15)$$

where  $\alpha_{0s}$  is a constant depending on the bare charge and temperature. Analogous arguments, involving the electrostatic potential  $\psi(r)$  calculated from the exact PB equation, establish the change in the short-range behavior of  $\psi(r)$  as a fingerprint of the counterion condensation phenomenon [10].

From the field theoretical approach [5, 6], it is expected that

$$\alpha_{0+} = \begin{cases} Z\Gamma & Z\Gamma < 2 - \Gamma \\ 2 - \Gamma & Z\Gamma > 2 - \Gamma \end{cases} \quad \alpha_{0-} = -Z\Gamma, \quad (16)$$

i.e. at  $Z\Gamma > 2 - \Gamma$  the coions interact with the guest charge as if the latter one carries a charge  $\hat{Z} = 2/\Gamma - 1 = Z_c - 1$  independent of  $Z$ , whereas the counterions always interact with the bare charge  $Z$  [5]. Figure 5 shows the values of  $\alpha_{0s}$  evaluated from the short-range values of  $g_{0s}(r)$ . In order to evaluate them, we carried out linear fits of  $\ln g_{0s}(r)$  according to (15). The comparison between the numerical results at  $\Gamma = 0.5$  to the ones given by (16) indicates that the short-range behavior of  $g_{0+}(r)$  when  $\kappa\sigma = 10^{-2}$  is qualitatively consistent with that of a system of point-like charges. However, from the figure it can be noted that as  $Z\Gamma \rightarrow 2$  a change in  $g_{0-}(r)$  is also found, as it was suggested in [5]. This fact indicates that as the coupling increases, the counterions “see” the guest charge with a smaller charge than  $Z$ . At this point, the effect produced by the correlation between the counterions jointly to the hard-disk potential provoke the increase of distance between the guest particle and the counterions. Also, as a consequence of this change at large enough coupling, the maximum value of  $Z_{ren}$  do not reach the saturation value predicted by PB theory, which is indicated in figure 4 through the dashed line at  $Z\Gamma > 2$ .

On the other hand, the charge accumulation around  $Z$  can be also measured through the integrated charge distribution

$$P(r) = -\frac{2\pi}{Z} \int_0^r \rho(r') r' dr' \quad (17)$$

where  $\rho(r) = (nz_+z_-)(g_{0+}(r) - g_{0-}(r))/(z_+ + z_-)$ .  $P(r)$  indicates the overall electric charge found within a disk of radius  $r$  and can be used to define the cutoff distance, the so-called Manning radius  $r_m$ , which separates the condensed



counterions from the uncondensed ones. According to a geometrical construction, the cutoff distance is identified by an inflexion point in  $P(r)$  when it is displayed as a function of  $\ln r$  [10, 11, 12], i.e.

$$P_{yy}(r)\Big|_{r=r_m} = \frac{d^2 P(r)}{d(\ln r)^2}\Big|_{r=r_m} = 0. \quad (18)$$

Figure 6 shows  $P(r)$ . As expected, at larger  $Z\Gamma$ , the short distance behavior of  $P(r)$  is dominated by the counterion density. Besides, as demonstrated before in the third panel of the figure 1 for which  $Z\Gamma = 3$  and  $\Gamma = 0.4$ , the onset of a peak in coion profile at high enough  $Z\Gamma$  and  $\Gamma$  does mark the extension of condensed counterions layer and give rise to inflection points in the integrated charge distribution.

The locus of points satisfying  $P_{yy}(r_{in}) = 0$  is plotted in figure 7. This figure shows that for all values of  $Z\Gamma$  an inflection point beyond the Debye length is found. This point represents a characteristic change of convexity of  $P(r)$  (as a function of  $\ln r$ ) induced by screening not by the condensed layer [12]; the inflection points associated with this layer appear when  $Z\Gamma \gtrsim 2$ . As it was mentioned above, for point-like particles it is expected that counterion condensation begins at  $2-\Gamma$ ; however, as consequence of finite radius of particles, the onset of inflection points for different values of  $\Gamma$  takes place at larger values, as can be inferred from figure 7. It is important to note that smallest values of  $r_{in}$  arise as an effect of the hard-disk radius, as becomes clearer from the inset.

As figure 7 shows, increasing  $\Gamma$  produces a thicker layer of condensed counterions, that is, the counterion condensation is enhanced as a consequence of increasing microions correlations. If the renormalized charge is considered as a result of the condensation phenomenon, then a smaller value of  $Z_{ren}\Gamma$  than the one predicted by PB theory is expected. It is indeed the case, as the figure 4 displays: at high enough  $Z\Gamma$ , the renormalized charge decreases as the bare charge increases because  $r_m$  becomes larger.

#### 4.1.2 Asymmetric TCP

In order to study the effects of the charge asymmetry on  $Z_{ren}$ , we carried out a similar analysis to the one presented in the previous section when particles forming the TCP are characterized by  $z_+ = 1$  and  $z_- = 1/2$ . If all particles were point-like, the stability region would be restricted to  $-2 < Z\Gamma < 4$ . We choose to work with these “valences” because, some exact results exist concerning the pair correlation functions of this kind of TCP [13, 14]. In this section, we consider both negative and positive values of  $Z$ , so that, in the cases when  $Z > 0$  and  $Z < 0$  we may refer to them as  $1:\frac{1}{2}$  and  $\frac{1}{2}:1$  cases, respectively.

Figure 8 shows the correlation functions between the microions at two different values of  $\Gamma$ . Due to our approximation, in the infinite dilution limit the correla-

tion functions  $g_{ss'}(r)$  are independent on  $Z$ . As it can be seen, at  $\Gamma = 0.2$  and  $\Gamma = 0.7$  the agreement between the numerically evaluated correlation functions  $g_{ss'}(r)$  and those predicted by field theoretical arguments in [13] (valid at large distances) is fairly good at large enough distance ( $\kappa r \gtrsim 0.5$  and  $\kappa r \gtrsim 1.5$ , respectively); this is particularly the case for  $g_{+-}(r)$  and  $g_{--}(r)$ . Additionally, the electroneutrality condition is fulfilled for this TCP. It was found that the zero moment defect was less than  $2 \times 10^{-3}$  for all values of  $Z$  and  $\Gamma$  reported in this section.

Figures 9 and 10 show plots of the correlation functions between the guest particle and the microions at different values of the bare charge for  $1:\frac{1}{2}$  and  $\frac{1}{2}:1$  cases, respectively. These curves were calculated for  $\Gamma = 0.2$  and  $\Gamma = 0.7$ . As it can be expected, the correlations between the guest particle and the counterions exhibit larger values when the latter ones have higher valence. It should be noted that the curves behave monotonically and do not cross for any coupling in case  $1:\frac{1}{2}$ ; the same happens at  $\Gamma = 0.2$  in  $\frac{1}{2}:1$  case. However, for the latter case at  $\Gamma = 0.7$  it is observed at larger  $Z$ , that the counterion profile near the guest particle (which is associated with  $g_{0+}(r)$ ) falls off much faster; also, the coions profile shows a peak at  $\kappa r \approx 0.1$ . As in the symmetric case, these facts suggest the presence of a counterion shell strongly bounded to the guest particle, which considerably screens the repulsion between the guest charge and the coions, and consequently plays an important role in the renormalized charge  $Z_{ren}$  setting.

As in the symmetric case, the renormalized parameters were evaluated by a linear fit of the functions  $L_{0\pm}(r)$  as those shown in figure 11, where the curves displayed were evaluated at  $\Gamma = 0.7$  and for different values of bare charge  $Z$ . In addition to the condition  $10^{-4} \leq |\log g_{0s}(r)| \leq 10^{-2}$ , in some cases it was mandatory to introduce empirically a minimum value of  $r$  in order to select an adequate range to be fitted. Such a situation was found particularly at large coupling and for  $Z < 0$ , where the correlation function between the guest charge and the coions exhibits a pronounced oscillation as it is shown in figure 11 for  $Z = -4$ .

Within the range of couplings explored,  $0.1 \leq \Gamma \leq 0.9$ , the renormalized inverse screening length  $\kappa_{ren}$  is found to be systematically larger than  $\kappa$ , and it is an increasing function of the coupling  $\Gamma$ , in agreement with the exact results [5]. Notice that this is the opposite behavior than the one found in the symmetric electrolyte. The ratio  $\kappa_{ren}/\kappa$  only differs from 1 by at most 3% for the largest coupling  $\Gamma = 0.9$ .

In figure 12, the renormalized charge resulting from the fitting procedure is illustrated as a function of  $Z$ . The global behavior of  $Z_{ren}$  shares much of the features described in [14], where an analysis based on the integrable complex Bullough-Dodd (cBD) model was used. The most remarkable outcome corresponds to  $\frac{1}{2}:1$  case at  $\Gamma \geq 0.8$ . In such a situation, we observe a very strong neutralization of  $Z_{ren}$  as  $|Z|\Gamma$  increases beyond 2, which gives rise to the charge

inversion phenomenon, i.e. the renormalized and bare charges have opposite signs.

Because of the asymmetry, the correlations between microions provoke an extra attraction of the counterions to, and repulsion of the coions from, the guest particle. This causes the accumulation of a large number of counterions around of the guest particle, as shown in figure 10, whose charge exceeds the amount necessary to neutralize  $Z$ . As it was mentioned, charge inversion is predicted by an exactly solved 2D model based on cBD theory [14]. However, it has also been reported in systems having other symmetries by using the HNC approximation [9, 15]. The decisive characteristic of the systems in which this process takes place is the asymmetry (either of size or charge) among coions and counterions. Particularly, when the ions are equally sized particles, it seems necessary that the counterions have larger valence (in absolute value) than the coions, as in the present situation.

The charge inversion phenomenon involves microions correlations and therefore the mean field PB treatment is not able to predict it. In addition to the charge inversion, in the case  $1:\frac{1}{2}$  the “overshooting” phenomenon predicted in [16], i.e. effective charge becomes larger than the bare charge for intermediate values of the latter one, is also observed. In such situation, coions are repelled further away in the double layer than they are in the symmetric case. The inset of figure 12 illustrates the comparison between HNC with PB results; the latter ones were obtained from ( $\sigma_0 = \sigma = 0$ ) [10]

$$Z_{ren}\Gamma = \frac{\sqrt{3}}{\pi} \left( 2 \sin \left( \frac{\pi Z\Gamma}{3} - \frac{\pi}{6} \right) + 1 \right). \quad (19)$$

Equation (19) is strictly valid when  $-1 < Z\Gamma < 2$ , i.e. if  $Z\Gamma$  does not exceed the Manning thresholds for counterion condensation, otherwise  $Z_{ren}\Gamma$  saturates to  $\frac{-\sqrt{3}}{\pi}$  and  $\frac{3\sqrt{3}}{\pi}$ , respectively [14].

As in the symmetric case, condensation thresholds mark the change of behavior of the correlation functions at short distance [14]. In figures 13 and 14 the short-range correlation functions and the  $\alpha_{0\pm}$  factors are plotted (see equation (15)). As before, the  $\alpha_{0\pm}$  factors determine the strength of the potential of mean force  $w_{0\pm}(r)$  between the guest particle and the microions at short distance. The curves were evaluated at  $Z = -3.6$  and for different values of the coupling parameter  $\Gamma$ . From the figure we can observe that there exists a point from which the interaction between the guest particle and the coions (i.e. negative ions) becomes less and less repulsive. As before, that change can be interpreted as a first step in the counterion condensation [14]. At  $\Gamma = 0.8$  that change is much more dramatic to the extent that the interaction begins to be attractive. Subsequent to the sign change in the short-range of  $w_{0-}(r)$ , the inversion of the renormalized charge (which is evaluated at large distance) takes place. On the contrary, the interaction between the guest charge and the counterions is hardly modified as  $|Z|$  increases, i.e. at all coupling parameters, the counterions seem

to “see” just the bare charge at short distance.

In order to study the thickness of the condensed layer we use again the inflection point criterion (18) for the integrated charge distribution  $P(r)$ . Figure 15 shows the locus of the inflection point for both  $\frac{1}{2}:1$  and  $1:\frac{1}{2}$  cases. In the first place, for the case  $1:\frac{1}{2}$  it is found that inflection points are located beyond the Debye length when  $\Gamma < 0.8$ . In this way, for the considered range of  $Z > 0$  the renormalized charge is well described by the PB approach at coupling strength below 0.8. On the other hand, when  $\Gamma \gtrsim 0.8$  and  $Z \gtrsim 4.5$  a new inflection point is detected at  $\kappa r_m \sim 0.1$ , i.e. at these bare charge and coupling parameters values the correlations give rise to the counterion condensation. Note that at such conditions the renormalized charge is close to reach its maximum value, as figure 12 suggests.

With regard to the  $\frac{1}{2}:1$  case, a richer scenario is found. For a large enough coupling, two inflection points are found, the smallest of them corresponding to  $r_m$ . As in the other cases, the onset of  $r_m$  is associated with coupling conditions at which the maximum (absolute) value of  $Z_{ren}$  is reached. Upon a further increase of  $|Z|$  these inflection points shift one toward the other and finally coalesce and annihilate, as it can be seen in figure 15. In addition, the bare charge at which such annihilation takes place,  $Z^*$ , is related to the onset of a peak in the coions density, i.e.  $g_{0-}(r)$ .

Within the cell model of polyelectrolytes, that annihilation occurs when the typical salt screening length (Debye length) interferes with the size of the condensed counterion layer and therefore it becomes unnecessary to distinguish between condensed and uncondensed counterions [12]. Moreover, it has been argued about the merit of the inflection point criterion, which unifies the phenomenology of an infinite dilution/finite salt system (as the studied one here) and that of the a finite density/vanishing salt cell model [10, 17]. However, our results suggest a different situation: because of the microions correlations, for  $Z > Z^*$  a second layer mainly constituted by coions starts to be formed at some distance of the guest particle.

On the other hand, according to the two-state model, the distribution of microions around the macroion can be divided into a condensed counterion region and a free population; the latter one being considered within the linearized PB theory. So, the role of a condensed layer is to impose a new boundary condition to the electric potential and consequently fixing the value of the renormalized charge [17]. However, since there is no inflection point of  $P(r)$  for  $Z > Z^*$ , we may not differentiate such populations at large enough coupling (i.e. strong microions correlations). In fact, the renormalized charge and subsequently the charge inversion are determined by a “layered” ionic cloud, as the insets in figures 10 and 15 suggest. An additional discussion about that “layered” cloud will be carried out later.

In this way, the process behind charge inversion appears to be a similar one to the secondary cause of the “Mechanism I” proposed in [15]. Since the net charge around the guest particle has opposite sign to that of  $Z$ , coions at some distance from the guest charge are attracted electrostatically towards the guest particle, while the counterions are repelled electrostatically from it, leading to the existence of a range of  $r$ -values at which the mobile ion system is locally oppositely charged, as figure 16 corroborates for  $\Gamma = 0.8$ .

## 4.2 Colloidal suspension at infinite dilution limit

As it was previously mentioned, 2D Coulomb systems can be used as a first approach to model some rod-like colloids and polyelectrolytes. Many synthetic as well as biological examples can be classified within this category. Depending on the number of charges per monomer unit bound to the backbone, the linear charge density  $\lambda$  can be tuned, so that typical dimensionless values comprise  $|\xi| = |\lambda|l_B = 3 - 6.6$ , where  $l_B$  is the Bjerrum length.

In order to study the effective charge in a little more realistic model of a cylindrical macroion immersed in an electrolytic solution, we follow similar assumptions to those given in [9] and [14]. At first, we consider a long charged cylindrical macroion with diameter  $a_0 = 20\text{\AA}$  immersed in an electrolytic solution composed by ions with diameter  $a = 5\text{\AA}$ , all of them interacting through a logarithmic potential. Temperature is fixed through the Bjerrum length  $l_B = 7.2\text{\AA}$ , which corresponds to aqueous suspensions at  $T = 293$  K. In order to study the effect of salinity we consider both symmetric (1:1) and asymmetric (1:2 and 2:1) electrolytes at different concentrations  $n$ .

By assuming the DH-like decay of the correlation functions  $g_{0\pm}(r)$  at large distances, we have obtained for the symmetric case the renormalized charge exhibited in figure 17. We found a qualitative behavior that resembles the one shown by the guest charge system. Again, the most significant difference between the HNC and analytical PB results [10] is the presence of a maximum value of  $\xi_{ren}$  followed by a monotonic decay in the HNC outcomes.

A similar dependence has been described for the zeta potential of a charged cylinder [18] and for the renormalized charge within a spherical cell model of ionic condensation [19, 20]. By using the density-functional theory based on a weighted (i.e. non-local) density approximation, the monotonic decrease of  $\xi_{ren}$  as  $\xi$  increases can be explained in terms of the excess chemical potential  $\mu_{exc}(r)$ . As  $\xi$  increase, the number of counterions is also increased due to the electroneutrality condition and therefore  $\mu_{exc}(r)$  near the particle surface decreases, resulting in an additional number of counterions attracted towards the surface [19]. In this way,  $\xi_{ren}$  must decrease when  $\xi$  surpasses the value where the maximum  $\xi_{ren}$ , which is as well related to the plateau predicted by

PB theory, is reached.

As before, the extent of the condensed counterion layer can be measured by using the integrated charge distribution (17). In figure 18 inflection points of  $P(r)$  are plotted as a function of the bare linear charge density for different salt concentrations. At high enough density ( $n > 0.05\text{M}$ ), the counterion condensation appears to occur at the macroion surface and involves a single layer of counterions. This layer is moderately bound to the charged cylinder, as it can be concluded by comparing the order of magnitude of  $g_{0-}(\sigma_c)$  at  $n = 0.001\text{M}$  to that at  $n = 0.1\text{M}$ . Beyond this region, the charge distribution is dominated by screening and falls off in a DH-like manner after approximately one Debye length, as it is shown in the inset of the figure 19.

At low density ( $n < 0.01\text{M}$ ),  $r_{in}$  depends on  $\xi$  in a similar way to what is shown in figure 15. For  $n = 0.001\text{M}$ , we can associate the smallest value of  $r_{in}$  to the Manning radius within the range  $1 \lesssim \xi \lesssim 3$ . Besides, that range roughly discriminates the region where  $\xi_{ren}$  passes from an increasing to a decreasing function, as it can be seen in figure 17. When  $\xi > 3.4$ , inflection points related to the finite size of microions enter to scene, indicating the accumulation of a second layer of counterions and consequently, the additional decrease in  $\xi_{ren}$ . Further increasing  $\xi$  produces annihilation of the inflexion points at  $\xi \approx 4$  and simultaneously  $g_{0+}(r)$  starts exhibiting a peak, as figure 19 illustrates.

Previously, when the charge inversion phenomenon was discussed, we associated the onset of a peak in the coions density profile to the settling on of a “layered” ionic cloud and we argued that the renormalized charge is determined by the net charge enclosed in that cloud (see figure 16). A similar conclusion has been given from the comparative study at very low ionic strength of the electrokinetic and the effective charges, which were obtained from electrophoresis and light scattering data of suspensions of latex particles, respectively [21].

According to the study carried out in [21], it may be stated that, interacting at large distance, colloidal particles act as if they carry an effective charge equal to the one enclosed by the so-called outer Helmholtz plane (OHP), from which the diffuse double layer begins. To a certain extent, the definition of OHP can be associated to the choice of the  $r$  value, from which  $g_{0+}(r)$  and  $g_{0-}(r)$  fall off symmetrically with respect to 1 in a DH-like form, i.e. the choice of an adequate range to fit correlation functions within the linearized theory. On the other hand, we would like to point out that the determination of the electrokinetic charge depends on the previous evaluation of the zeta potential and, as it was aforementioned, the behavior of  $\xi_{ren}$  shown in figure 17 and that of the zeta potential for a charged cylinder found in [18] are qualitatively similar. In this way, our results suggest that the HNC approach captures appropriately, at least qualitatively, the short-range correlations determining the double layer structure.

On the other hand, when the macroion is immersed in an asymmetric electrolyte composed by divalent and monovalent ions, the renormalized charge evaluated from HNC calculation behaves as shown in figure 20. Again, the overshooting and charge inversion phenomena are observed. In the 2:1 case at  $n = 5 \times 10^{-4}\text{M}$  ( $\kappa\sigma_c \approx 0.09$ ) and  $n = 0.001\text{M}$  ( $\kappa\sigma_c \approx 0.13$ ), figure 21 suggests the presence of a well defined layer of condensed counterions. At these densities, the Manning radius dependence on  $\xi$  is qualitatively similar to the one predicted by PB theory; however, it appears to underestimate the thickness of the condensed layer. If we would consider the renormalized charge as the net charge enclosed by the Manning radius (two-state model), then the renormalized charge should be smaller than the bare one, and therefore, the overshooting phenomenon would not be present.

In spite of a thicker condensed layer, depending mainly on short-range correlations between the macroion and the counterions, the HNC approach also predicts overshooting. This phenomenon lies in the fact that divalent coions are expelled further away in the double layer than the monovalent ones in the 1:1 situation, which results in a stronger electrostatic potential at larger distance [16]. Although the PB theory accounts for this phenomenon, figure 20 shows that the mean field solution underestimates the magnitude of the overshooting effect as well as the range of  $\xi$  where it is present, which is particularly notorious at high density.

Likewise, at high enough density (for instance,  $n = 0.005\text{M}$  ( $\kappa\sigma_c \approx 0.29$ )), as  $\xi$  increases the Manning radius increases faster than its PB counterpart (dashed line in figure 21) and eventually fuses with the inflection point characterizing the salt. Again, when inflection points are close enough, a peak in  $g_{0+}(r)$  appears, i.e. a local increase of coions density takes place, as it can be seen in the bottom frames of figure 22. In these circumstances, the Manning inflection point and the Debye length become comparable so that, the charge renormalization is determined by a more correlated ionic cloud giving place to a saturation value of  $\xi_{ren}$  within the studied range of  $\xi$ , as it is displayed in figure 20.

With respect to the 1:2 case, the differences between PB and HNC results become more significant. For all the considered densities, soon after the linear charge density is larger (in absolute value) than the Manning condensation threshold ( $\xi_m = -0.5$ ), the renormalized charge decays quickly to zero and gets the positive sign at  $\xi \lesssim -1.3$  (see the inset of figure 20). As well, there is no qualitative similarity in the Manning radius evaluated from both of those approaches, suggesting that the short-range correlations between macroions and microions play a more predominant role in this situation. Although in figure 22 the coion densities for both 1:2 and 2:1 electrolytes exhibit a qualitatively similar behavior as  $|\xi|$  increases, we call the attention on the difference between their orders of magnitude at  $r = \sigma_c$ : in the 2:1 case the first microion layer around the macroion corresponds only to counterions whereas in the 1:2 case, this appears to be conformed both of counter- and coions. This fact indicates a change in

the short range behavior of the mean force potential between the macroion and the coions, as it was mentioned earlier. In the 1:2 case, increasing further  $|\xi|$ , the counterion fraction of the ionic cloud around the macroion does not only compensates for its total charge but even exceeds it, giving rise to a charge inversion phenomenon, as it is displayed in the inset of figure 20.

Also, the results show the existence of a maximum value of the effective charge  $\xi_{ren}^{max}$ . In order to describe the dependence of that maximum on the macroion radius  $\sigma_0$ , we evaluate  $\xi_{ren}$  at different values of  $\sigma_0$  for both symmetric and asymmetric electrolytes. The outcome of these calculations within the HNC convergence range are shown in figures 23 and 24. As it can be seen, the qualitative behavior appears to be the same previously discussed: the observation of the maximum of  $\xi_{ren}(\xi)$  followed by a monotonic decrease is systematically found in all studied cases. In figure 25, the dependence of the maximum of  $\xi_{ren}$  on the reduced radius  $\kappa\sigma_c$  ( $\sigma_c = \sigma_0 + \sigma$ ) is displayed. Although systematically lesser,  $\xi_{ren}^{max}$  qualitatively follows the same tendency (at least within the considered range) that the saturation value from PB theory ( $\xi_{sat}^{PB}$ ) at  $\kappa\sigma_c > 1$  in both symmetric and asymmetric electrolyte [16, 22]. We can associate the  $\xi_{ren}^{max}$  to the counterion condensation in the sense that, around the bare charge  $\xi^*$  at which the maximum is reached, the renormalized charge is mainly fixed by the macroion-counterion correlation. In this sense, since we use a 2D system, which overestimates correlations between microions, figures 25 can be used to establish both upper (PB theory, no microion correlations) and lower bound to the exact value of  $\xi_{ren}^{max}$ .

Finally, coming back to the figure 23 for  $n = 0.01M$  and  $\sigma_0 = 25\text{\AA}$ , a particular behavior of  $\xi_{ren}$  is found as  $\xi \gtrsim 15$ . At such conditions the decrease of  $\xi_{ren}$  appears to be less pronounced than the one found for  $8 < \xi < 15$ . This fact would indicate the eventual appearance of a plateau region in  $\xi_{ren}$  at large enough  $\xi$ ; nevertheless, since the HNC calculation does not converge at  $Z \gtrsim 16$ , it is difficult to give a conclusive argument in this direction.

## 5 Conclusions

We have evaluated the renormalized charge in a 2D system formed by a central charged particle (macroion) immersed in an electrolytic solution. By solving numerically the Ornstein-Zernike equations within the framework of the hypernetted chain approximation (HNC), we have calculated the correlation functions between the macroion and the microions ( $g_{0\pm}(r)$ ). Under the assumption that the correlation functions fall off exponentially, we found the renormalized charge by fitting the asymptotic behavior of the correlation functions to the one derived from the linearized PB theory (Debye-Hückel limit). The adequacy of this procedure was proved by comparing the numerical results to the analytical ones



from exactly solved 2D models.

The 2D model could be applied to study a cylindrical macroion immersed in an electrolyte formed by cylindrical co- and counterions, for instance, charged stiff polymers. Moreover, since particles in the model interact through a logarithmic potential, it would be expected that it preserves aspects concerning the nature of the Coulomb interaction, i.e., in a 3D model, the dependence of the renormalized charge on the bare one would share the same qualitative characteristics that those described here.

Recently, by using the theory of integrable systems, some analytical results concerning the renormalized charge within the non-linearized Poisson-Boltzmann (PB) theory have been reported [10]. The results of this work show that the renormalized charge is not explained qualitatively by the PB theory. As the bare charge of the macroion increases sufficiently, the PB theory predicts a constant value of the renormalized charge; on the contrary, the HNC renormalized charge reaches a maximal value and then monotonically decreases, both in symmetric and asymmetric electrolytes. This behavior takes place because the HNC approach appreciates the difference between the potential and the potential of mean force, which is exactly what the Poisson-Boltzmann theory neglects.

On the other hand, the structure of the ionic cloud around the macroion, which provokes the charge renormalization, can be described through either the density profiles  $g_{0\pm}(r)$  or the inflection points of the integrated charge density  $P(r)$  (defined by eq. (17)). For a weakly charged cylinder, the short range behavior of the potential of mean force between macroion and microions appears to correspond to the Coulomb interaction. Also, there is one inflection point associated to the screening phenomena in the bulk of the salt. Consequently, at that limit, the density profiles suggest a diffuse cloud, which gives rise to a linear screening that can be described by the Debye-Hückel approximation.

At low density, as the bare charge  $\xi$  increases, the stronger accumulation of counterions around the central particle results in a change of the short-distance behavior of the potential of mean force between macroion and coions, which has been interpreted as a precursor of the (Manning) counterion condensation [5]. Simultaneously, according to the inflection point criterion, a new inflection point at  $r_m < \kappa^{-1}$  can be identified. This point can be associated to the Manning radius provided that the bare charge is close to the Manning threshold; in such situation the renormalized charge is mainly fixed by the macroion-counterion correlation. Besides, since the maximum of the renormalized charge ( $\xi_{ren}^{max}$ ) exhibits the same characteristics as the plateau of the PB theory, it can be assumed that under these circumstances, the thermal energy of a counterion is nearly compensated by the reversible work required to remove it from the vicinity of the macroion.

On the other hand, by studying  $\xi_{ren}^{max}$  within an intermediate range of reduced

radius ( $10^{-2} < \kappa\sigma_c \lesssim 1$ ), we can conclude that  $\xi_{ren}^{max}$  as a function of  $\kappa\sigma_c$  is systematically smaller and present the same qualitative behavior than the saturation value of the PB theory. Since in our model the microions interact through a logarithmic potential, the role of microion correlations has been overestimated from the point of view of 3D systems. In this way, our HNC results could be established as lower bounds for the real  $\xi_{ren}^{max}$ .

As  $\xi$  increases further,  $r_m$  becomes bigger until it fuses with the inflection point characterizing the electrolyte. Under such circumstances, most of the counterions are located at the cylinder surface, whereas the rest of the screening charge, is spread in the ionic cloud. Nevertheless, the merging of the inflection point is related to the onset of a peak in the coions density profile. This suggests that beyond the counterion layer, the ionic cloud is not a diffuse layer which can be handled by means of the linearized theory, as the two-state model claims, but a more complex structure is settled by correlations between microions.

If we consider an asymmetric 1:2 electrolyte, the net charge in the vicinity of the cylinder surface has opposite sign to that of the bare charge. This fact causes that the coions at some distance from the surface to be attracted towards the macroion (giving rise to the mentioned peak) and that the counterions to be repelled from the macroion, leading to a reversion of the charge distribution in a region some distance from the cylinder. In this way, the evaluation of the renormalized charge from the asymptotic behavior of  $g_{0\pm}(r)$  allows to account for the charge inversion phenomenon without additional assumptions, in contrast to PB theory, in which the introduction of the counterion binding conjecture becomes necessary.

Therefore, the present study suggest that the HNC approach is able to take into account, at least qualitatively, the behavior of correlations responsible for the counterion condensation process, as well as the charge inversion one. As well, it gives indications in order to obtain a better description of the charge renormalization, because it intrinsically explains for the structure of the electric double layer. So, a theoretical method to estimate more adequately the renormalized charge at high enough  $\xi$ , must consider a more detailed description of the electric double layer structure by taking into account short range correlations between macro- and microions and between the last ones (for instance, density functional or dressed-ion theories).

Finally, a question remain to be solved: Does  $\xi_{ren}$  always continue to decrease at large  $\xi$ ? A unique of the outcomes presented in this work appears to indicate the possibility of a plateau region in  $\xi_{ren}$  at large enough  $\xi$ ; however, due to the non convergence of HNC calculation at high  $\xi$ , we cannot categorically state this conclusion. As it was mentioned, HNC approach is inadequate to treat the ion clustering effects, which could be of extreme importance at such a strong coupling. A device to overcome this difficult might be the introduction of a bridge function, which takes indirectly into account correlations mediated by

two or more particles.

This work was partially supported by a ECOS Nord/COLCIENCIAS action of French and Colombian cooperation.

## References

- [1] L. Belloni. 2000. Colloidal interactions. *J. Phys.: Cond. Matt.* **12**: R549–R587.
- [2] C. Likos. 2001. Effective interactions in soft condensed matter physics. *Phys. Rep.* **348**: 267–439.
- [3] L. Šamaj. 2005. Anomalous effects of “guest” charges immersed in electrolyte: Exact 2D results. *J. Stat. Phys.* **120**: 125–146.
- [4] L. Šamaj. 2006. Renormalization of hard-core guest charges immersed in two-dimensional electrolyte. *J. Stat. Phys.* **124**: 1179–1206.
- [5] G. Téllez. 2006. Guest charges in an electrolyte:renormalized charge, long- and short-distance behavior of the electric potential and density profiles. *J. Stat. Phys.* **122**(4): 787–98.
- [6] G. Téllez. 2005. Short-distance expansion of correlation functions in the charge-symmetric two-dimensional two-component plasma: Exact results. *J. Stat. Mech.* P10001
- [7] M. Guizar and J. Gutiérrez. 2004. Computation of quasi-discrete Hankel transforms of integer order for propagating optical wave fields. *J. Opt. Soc. Am. A.* **21**: 53–57.
- [8] F. H. Stillinger and R. Lovett. 1968. General Restriction on the Distribution of Ions in Electrolytes. *J. Chem. Phys.* **49**: 1991–1994.
- [9] D. Leger and D. Levesque. 2005. Effective interactions in the colloidal suspensions from hypernetted-chain theory. *J. Chem. Phys.* **123**: 124910–124920.
- [10] G. Téllez and E. Trizac. 2006. Exact asymptotic expansions for the cylindrical Poisson-Boltzmann equation. *J. Stat. Mech.* P06018
- [11] L. Belloni. 1998. Ionic condensation and charge renormalization in colloidal suspensions. *Colloids and Surfaces A.* **140**: 227–243.
- [12] M. Deserno, C. Holm and S. May. 2000. The fraction of condensed counterions around a charged rod: comparison of Poisson-Boltzmann theory and computer simulations. *Macromolecules.* **33**: 199–206.

- [13] L. Šamaj. 2003. Exact solution of a charge-asymmetric two-dimensional Coulomb gas. *J. Stat. Phys.* **111**(1-2): 261–290.
- [14] G. Téllez. 2006. Charge inversion of colloids in an exactly solvable model. *Europhys. Lett.* **76**: 1186–1192.
- [15] H. Greberg and R. Kjellander. 1998. Charge inversion in electric double layers and effects of different sizes for counterions and coions. *J. Chem. Phys.* **108**: 2940–2953.
- [16] G. Téllez and E. Trizac. 2004. Nonlinear screening of spherical and cylindrical colloids: the case of 1:2 and 2:1 electrolytes. *Phys. Rev. E.* **70**: 0114041–0114049.
- [17] B. O’Shaughnessy and Q. Yang. 2005. Manning-Oosawa counterion condensation. *Phys. Rev. Lett.* **94**: 0483021–0483024.
- [18] E. Gonzales-Tovar, M. Lozada-Cassou and D. Henderson. 1985. Hypernetted chain approximation for the distribution of ions around a cylindrical electrode II. *J. Chem. Phys.* **83**: 361–372.
- [19] R.D. Groot. 1991. Ion condensation on solid particles: Theory and simulation. *J. Chem. Phys.* **95**: 9191–9203.
- [20] W.L Hsin, T.Y. Wang, Y.J. Sheng and H.K. Tsao. 2004 Charge renormalization of charged spheres based on thermodynamic properties. *J. Chem. Phys.* **121**: 5494–5504.
- [21] M. Quesada-Pérez, J. Callejas-Fernández and R. Hidalgo-Álvarez. 1999. Renormalization processes in the charge density of polymer colloids. *Colloids and Surfaces A.* **159**: 239–252.
- [22] M. Aubouy, E. Trizac, L. Bocquet. 2003. Effective charge versus bare charge: an analytical estimate for colloids in the infinite dilution limit. *J. Phys. A: Math. Gen.* **36**: 5835–5840.

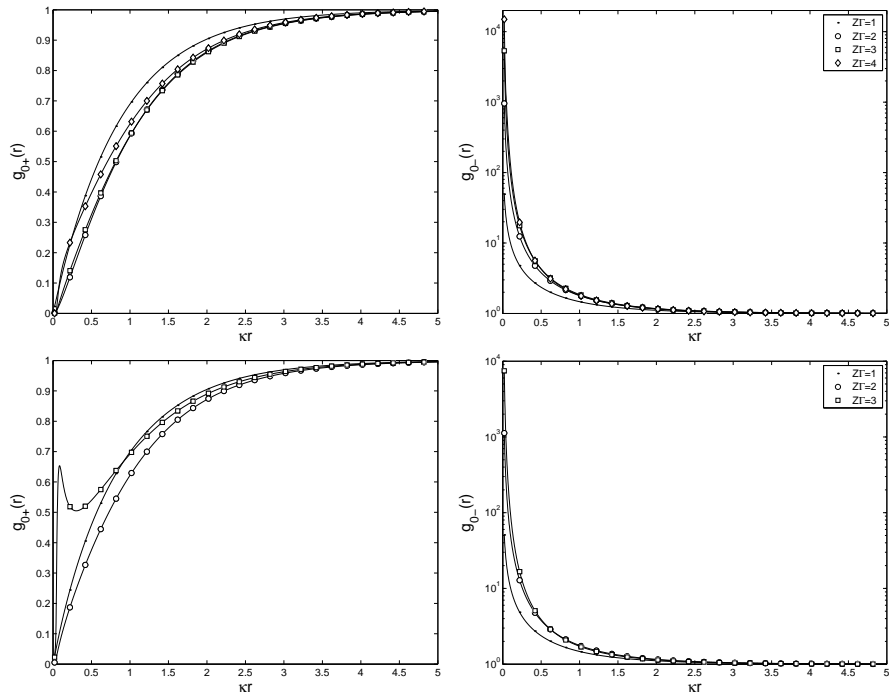


Figure 1: Correlation functions  $g_{0\pm}(r)$  at different values of  $Z\Gamma$  for a guest charge immersed in a symmetric TCP with coupling parameters  $\Gamma = 0.2$  (top) and  $\Gamma = 0.4$  (bottom).

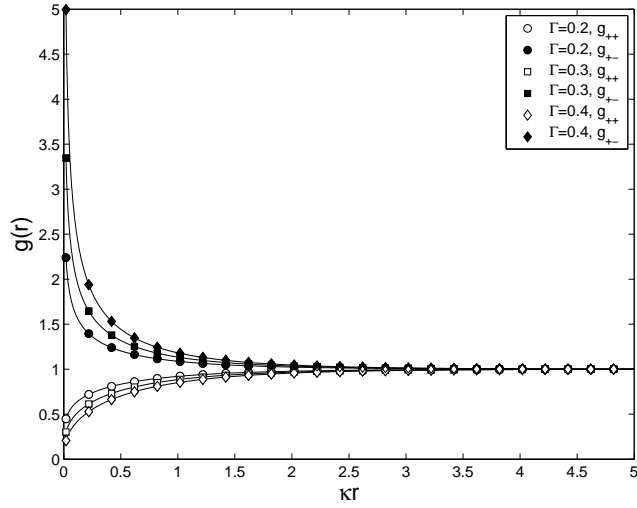


Figure 2: Correlation functions between microions of the symmetric TCP at different values of coupling parameter  $\Gamma$ . The plotted functions correspond to the ones evaluated when  $Z\Gamma = 3$ ; however these functions are independent of the magnitude of  $Z\Gamma$ , as expected from the equations (3)–(8).

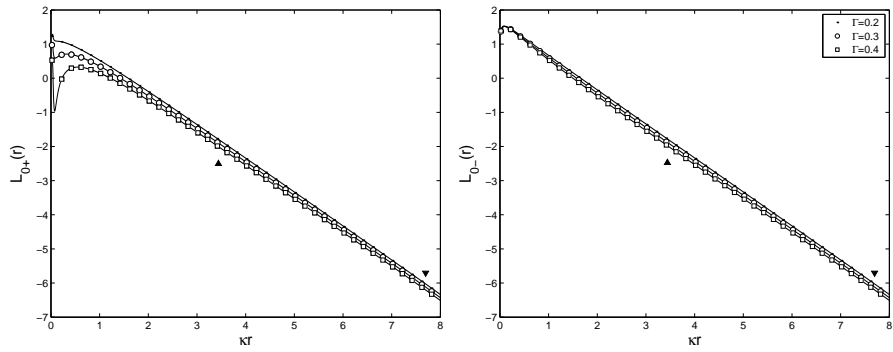


Figure 3: Functions  $L_{0\pm}(r)$  used to evaluate renormalized parameters. The curves were calculated from the correlation functions at  $Z\Gamma = 3$ . Triangles delimit the  $r$  range used for the linear fit.

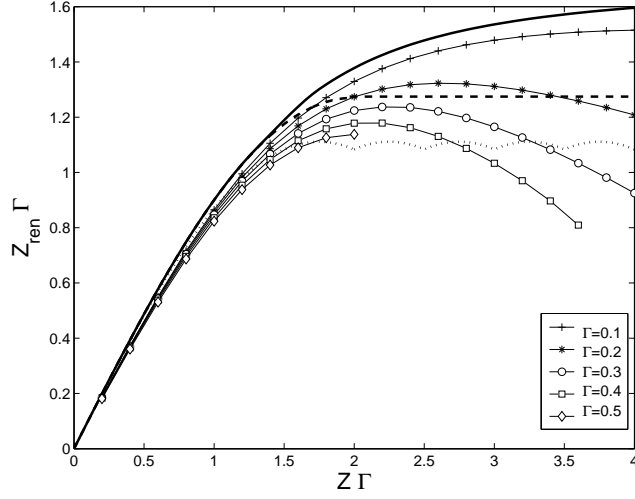


Figure 4: Renormalized charge as a function of the bare one for different coupling parameters. Dashed and thick continuous lines represent the mean-field PB analytical result for  $\sigma_0 = \sigma = 0$  and the numerical one when  $\kappa\sigma_0 = 10^{-2}$ ,  $\sigma = 0$ , respectively [5]. Dotted line indicates the exact result from field theoretical arguments ( $\kappa\sigma_0 \rightarrow 0$ ,  $\sigma = 0$ ,  $\Gamma = 0.5$ ) [4].



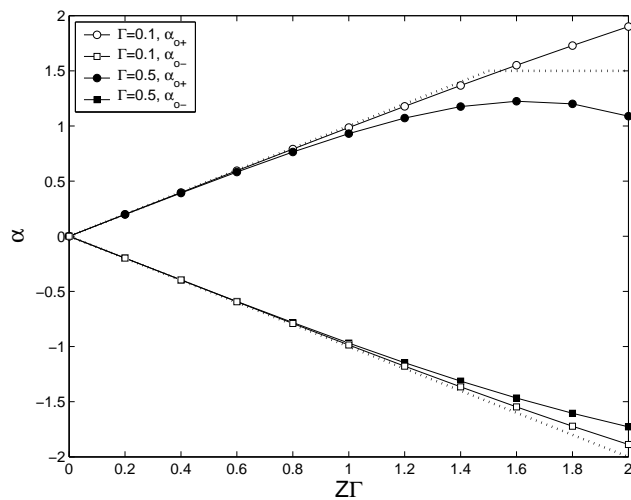


Figure 5:  $\alpha_{0s}$  factors characterizing the short-distance potential of mean force at  $\Gamma = 0.1$  and  $\Gamma = 0.5$ . In order to exclude the hard-disk effect, the data shown was calculated from a linear fit of  $\ln g(r)$  at  $6\sigma < r < 10\sigma \approx 0.1\kappa^{-1}$ . Dotted lines represent theoretical limits (16) at  $\Gamma = 0.5$ .

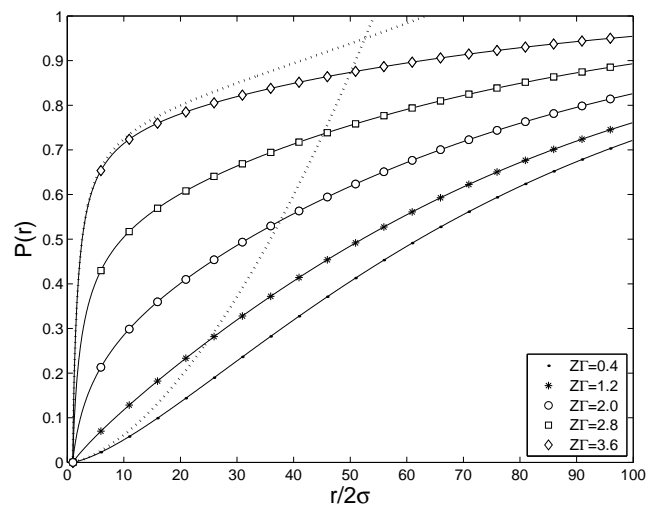


Figure 6: Integrated charge distribution as a function of the radial distance at  $\Gamma = 0.4$  and different values of  $Z\Gamma$ . Dashed lines represent the distribution of counterions when  $Z\Gamma = 0.4$  and  $Z\Gamma = 3.6$ . Radial range corresponds to two Debye lengths.

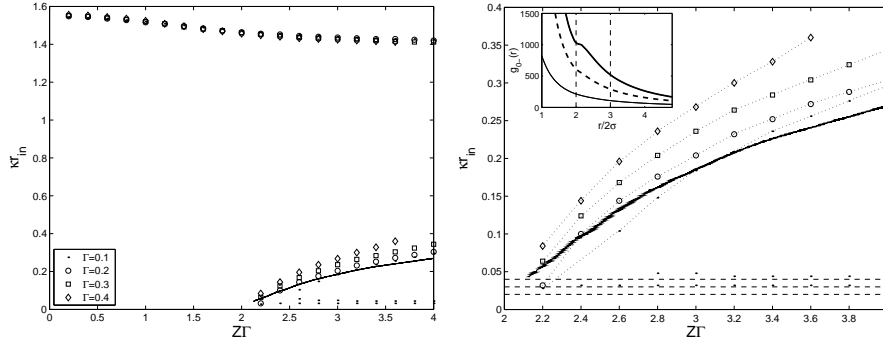


Figure 7: Inflection points of the charge distribution as a function of  $Z\Gamma$  for different values of  $\Gamma$  (left). Continuous line correspond to the numerical solution of PB equation (data taken from [10]). Detailed plot showing the Manning radius  $r_m$  (right). In the inset are shown the correlation functions  $g_{0-}(r)$  at  $\Gamma = 0.1$  for  $Z\Gamma = 2, 3, 4$ , which suggest that the onset of a well-defined second layer of counterions provoking smaller values of  $r_{in}$ . Thin dashed lines indicate the position of one, two and three particle diameters. Dotted lines are a guide to the eye.

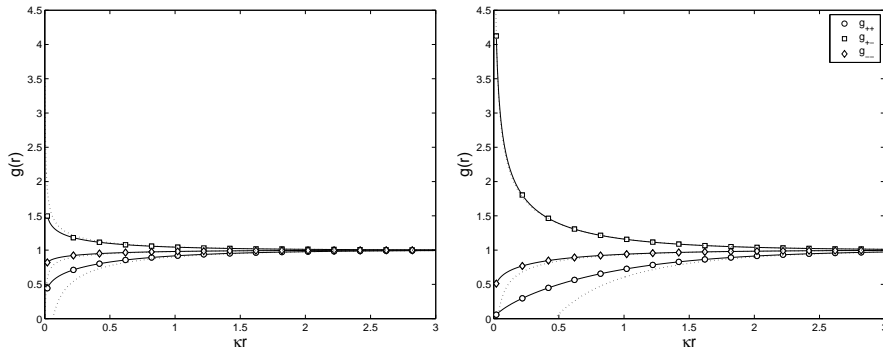


Figure 8: Correlation functions between microions at  $\Gamma = 0.2$  (left) and  $\Gamma = 0.7$  (right) for the asymmetric TCP. Dotted lines denote theoretical asymptotic limits given by field theoretical arguments [13].

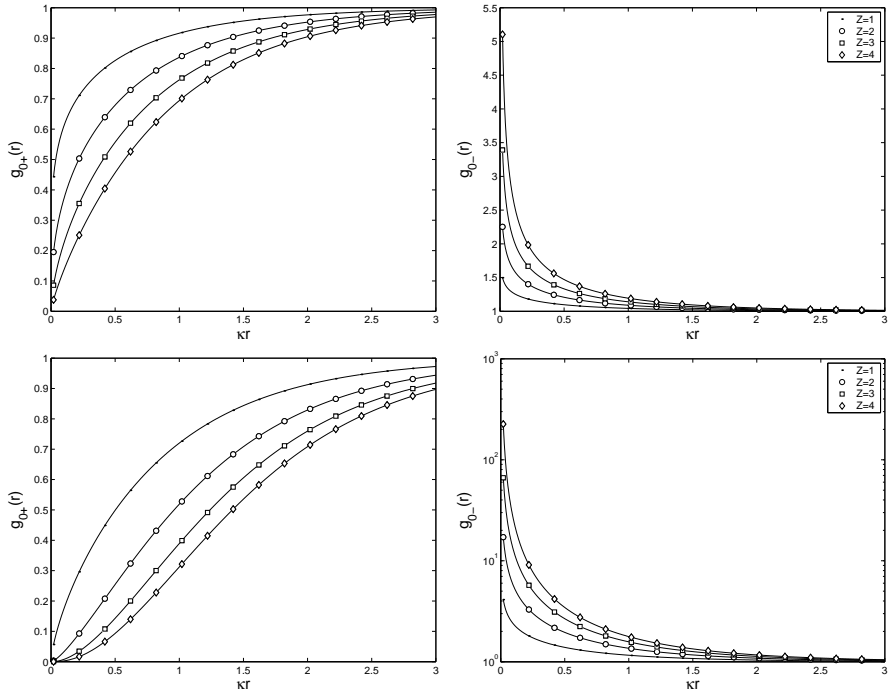


Figure 9: Correlation functions  $g_{0\pm}(r)$  for a guest charge immersed in an asymmetric TCP for different values of  $Z > 0$  ( $1:\frac{1}{2}$  case). The curves were evaluated at  $\Gamma = 0.2$  (top) and  $\Gamma = 0.7$  (bottom).

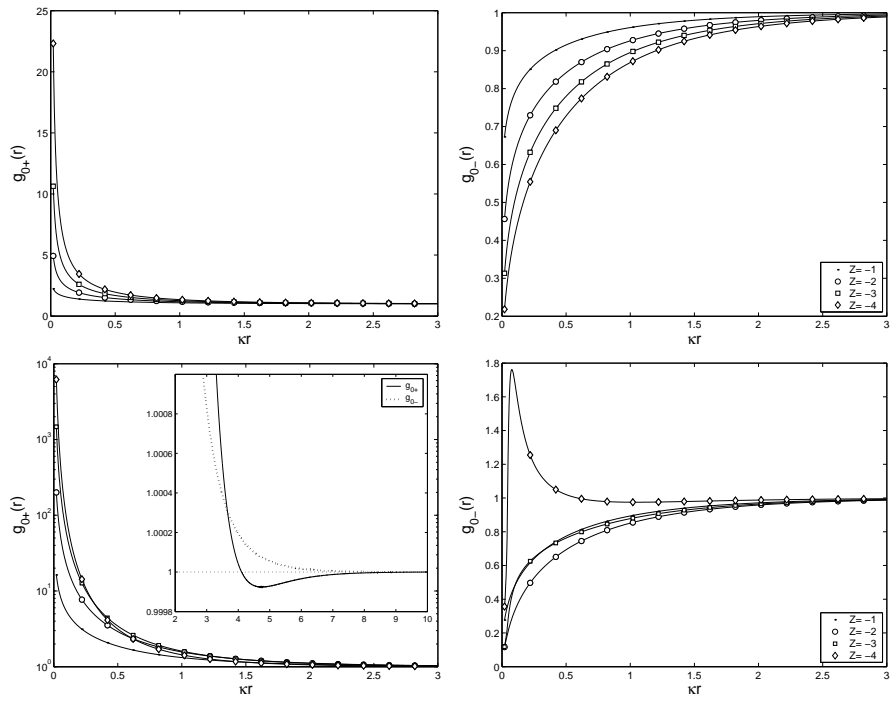


Figure 10: Same as the figure (9) but  $Z < 0$  ( $\frac{1}{2}:1$  case). The inset shows a detail of  $g_{0\pm}(r)$  for  $Z = -3.6$  and  $\Gamma = 0.8$ .

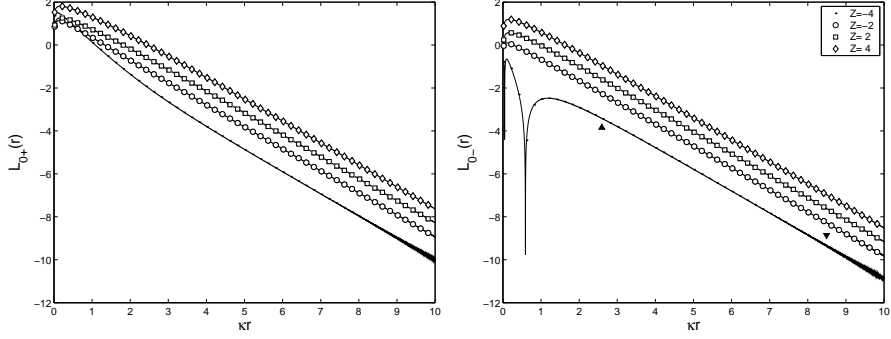


Figure 11: Functions  $L_{0\pm}(r)$  used to evaluate renormalized parameters. The curves were calculated from the correlation functions at  $\Gamma = 0.7$ . Triangles delimited the range of  $r$  according to  $10^{-4} \leq |\log g_{0s}(r)| \leq 10^{-2}$  for  $Z = -4$ .

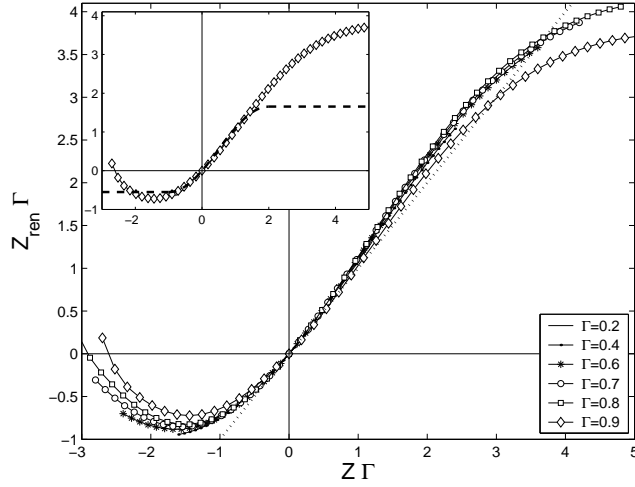


Figure 12: Renormalized charge for a guest charge immersed in an asymmetric TCP at different coupling parameters. Dotted line indicates the condition  $Z_{ren} = Z$ . In the inset the HNC result for  $\Gamma = 0.9$  is compared to the one predicted by PB theory (dashed line).

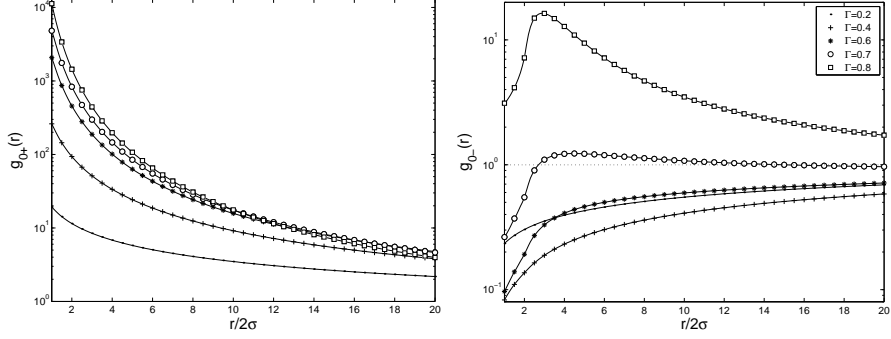


Figure 13: Short distance behavior of correlation functions  $g_{0\pm}(r)$  for  $Z = -3.6$  and different coupling parameters.

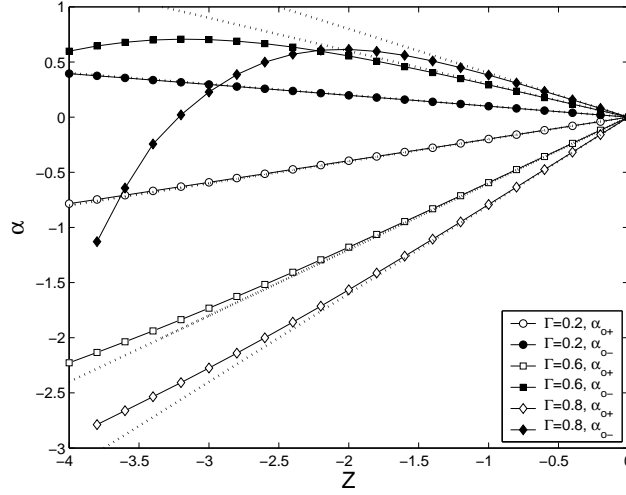


Figure 14:  $\alpha_s$  factors characterizing the short-distance behavior of the potential of mean force for different values of  $\Gamma$ . Dotted lines indicate factors related to the Coulomb potential ( $|\alpha_{0\pm}^{(coul)}| = |Z z_{\pm} \Gamma|$ ).

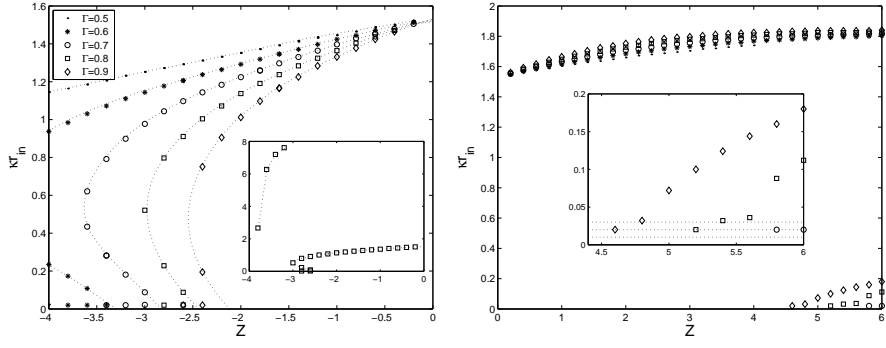


Figure 15: Inflection points of charge distribution as a function of  $Z$  and  $\Gamma$  for  $\frac{1}{2}:1$  (left) and  $1:\frac{1}{2}$  (right) cases. At the left, the inset shows an additional inflection point at larger distance when  $\Gamma = 0.8$ , which is related to the charge inversion. Dotted lines were obtained by interpolation but are intended as a guide to eye. As in the symmetric case, the smallest values of  $r_{in}$  are related to the finite radius of particles, as dotted lines indicate in the inset at the right.



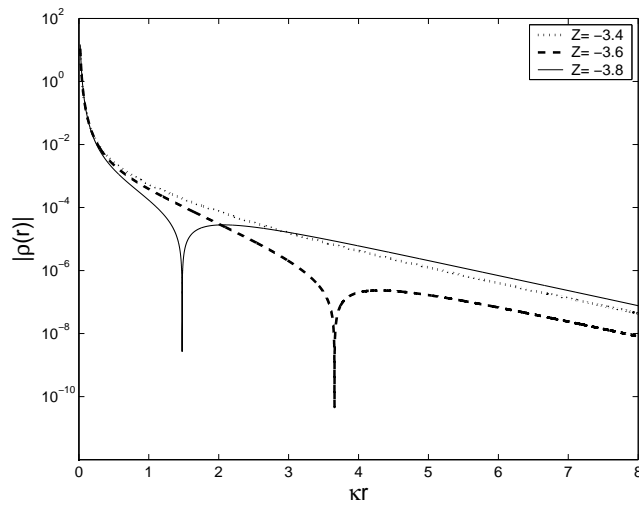


Figure 16: Absolute value of the charge density around guest particle for the  $\frac{1}{2}:1$  case at  $\Gamma = 0.8$ . Peaks indicate a change of sign of  $\rho(r)$  and therefore a change of sign in the renormalized charge. Note that the onset of such peaks imposes a restriction on the  $r$ -range used to the fitting procedure.

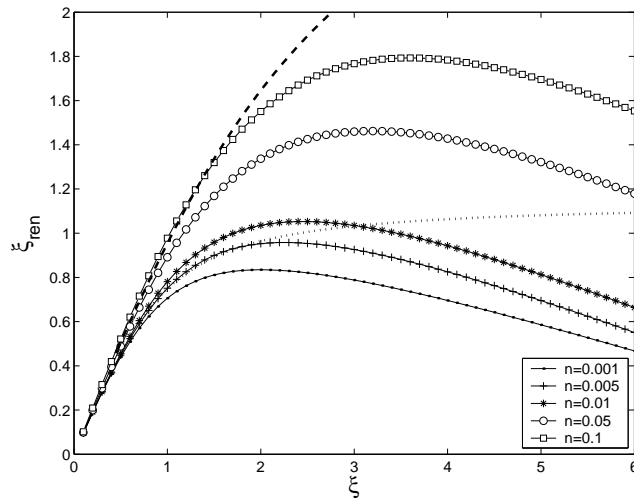


Figure 17: Dependence on the salinity of the renormalized charge for a charged cylinder immersed in a 1:1 electrolyte ( $[n] = M$ ). The renormalized linear charge density is compared to the exact PB results for  $n = 0.001M$  ( $\kappa\sigma_c \approx 0.074$ , dotted line) and  $n = 0.1M$  ( $\kappa\sigma_c \approx 0.74$ , dashed line).

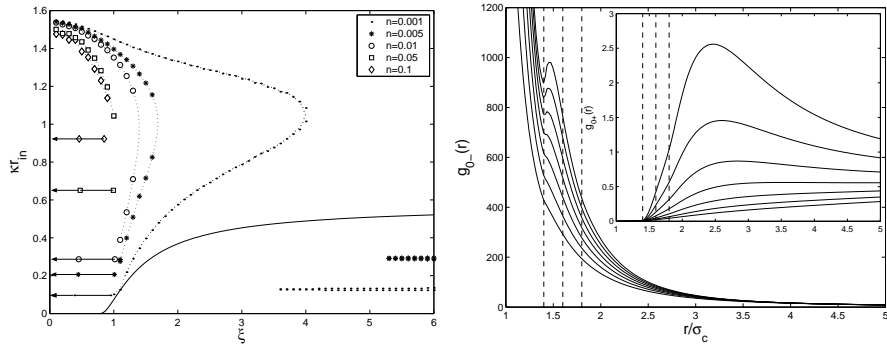


Figure 18: Inflection points in the integrated charge distribution (left). Arrows indicate values of  $\kappa\sigma_c$  for each density ( $[n] = M$ ). Dotted lines are intended as a guide to the eye; the continuous line indicates the exact PB result for  $n = 0.001$  ( $\kappa\sigma_c \approx 0.074$ ) [10]. At the right are shown the correlation functions  $g_{0\pm}$  for  $\xi = 3 \rightarrow 6$  at  $n = 0.001M$ . At higher values of  $\xi$ , the correlation functions exhibit inflection points as a consequence of finite radius of microions, which suggest the formation of a second layer of counterions.

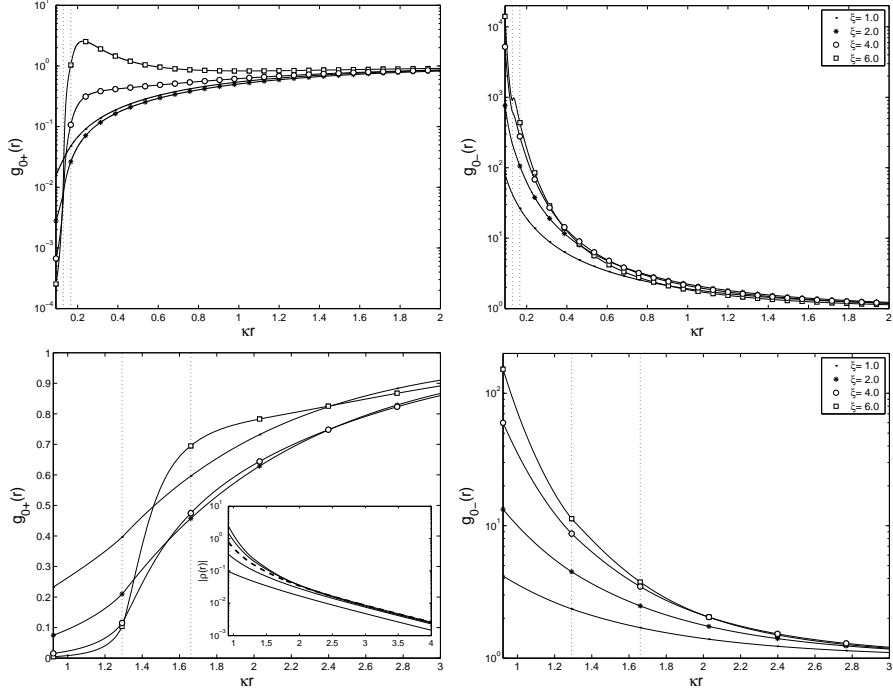


Figure 19: Correlation functions  $g_{0\pm}(r)$  at  $n = 0.001\text{M}$  (top) and  $n = 0.1\text{M}$  (bottom) for a cylindrical macroion. Dotted lines delimit the region  $r = \sigma_c + 2\sigma$  and  $r = \sigma_c + 4\sigma$ . When  $n = 0.001\text{M}$  and  $\xi = 4$ , the onset of a peak in  $g_{0+}(r)$  takes place. This point is associated with the annihilation of inflection points (see the figure (18)). In the inset is shown the charge density at  $n = 0.1\text{M}$  for  $\xi = \{1, 2, 3, 4, 5\}$  (dashed line indicates  $\xi = 3$ ).

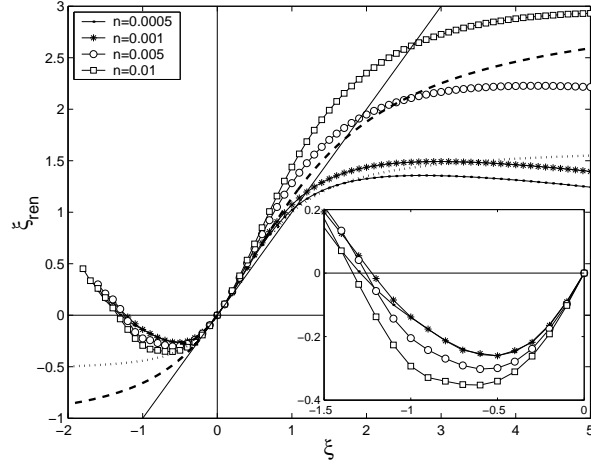


Figure 20: Renormalized charge for a cylindrical macroion immersed in an asymmetric electrolyte at different salinities. Dotted and dashed lines indicate analytical PB solutions at  $n = 0.0005\text{M}$  ( $\kappa\sigma_c \approx 0.9$ ) and  $n = 0.01\text{M}$  ( $\kappa\sigma_c \approx 0.41$ ), respectively.

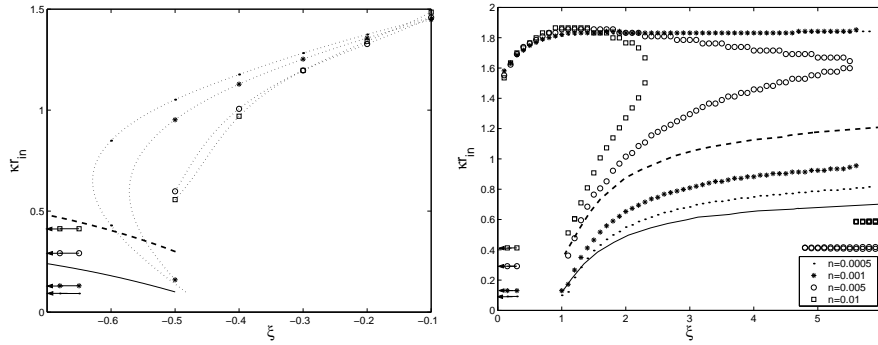


Figure 21: Locus of the inflection points of  $P(r)$  for a charged cylinder of radius  $\sigma_0 = 10\text{\AA}$  immersed in an 1:2 (left) and 2:1 (right) electrolyte. Continuous and dashed lines correspond to calculation of  $\kappa r_m$  by solving the PB equation for  $\kappa\sigma_c = 0.1$  and  $\kappa\sigma_c = 0.3$ , respectively [10]. Note that for  $n = 0.0005\text{M}$  and  $n = 0.005\text{M}$  correspond  $\kappa\sigma_c \approx 0.09$  and  $\kappa\sigma_c \approx 0.29$ , respectively. Arrows indicate the  $\kappa\sigma_c$  limits.

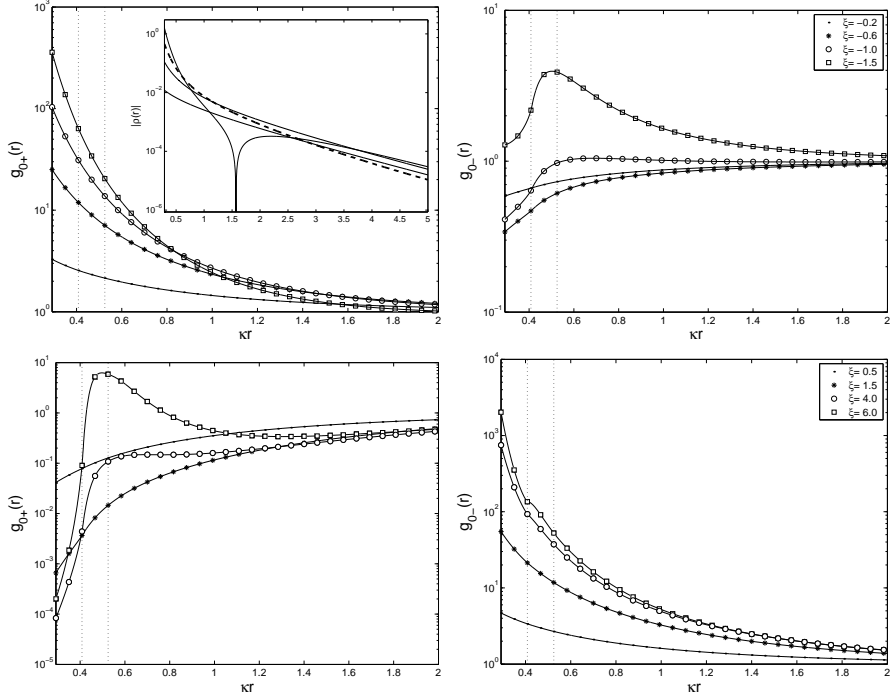


Figure 22: Correlation functions  $g_{0\pm}(r)$  for 1:2 (top) and 2:1 case (bottom) at  $n = 0.005M$ . In the inset are shown the associated charge densities (dashed line is used for  $\xi = -1.0$ ). Dotted lines marks  $r = \sigma_c + 2\sigma$  and  $r = \sigma_c + 4\sigma$ .

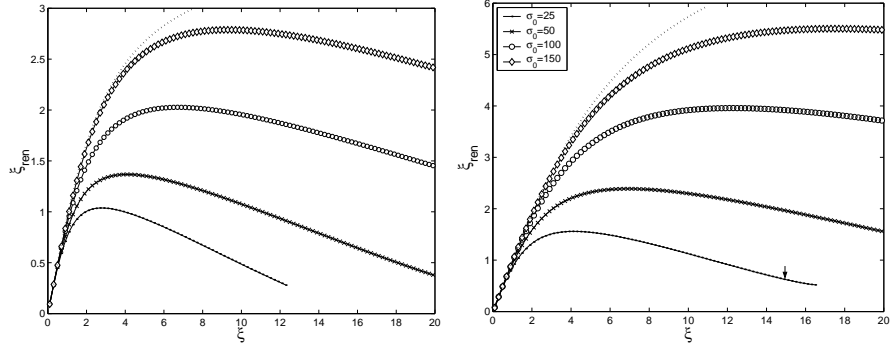


Figure 23: Renormalized charge in the symmetric case for different values of colloid radius ( $[\sigma_0] = \text{Å}$ ) at  $n = 0.001M$  (left) and  $n = 0.01M$  (right). Dotted lines indicate the PB solutions from [16] for  $\sigma_0 = 150\text{Å}$  ( $\kappa\sigma_c \approx 1.6$  and  $3.6$ , respectively). Arrow indicates a value of  $\xi$  from which a less pronounced decrease is apparently found.

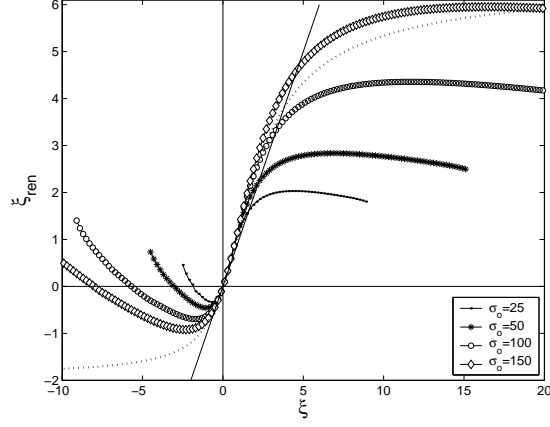


Figure 24: Renormalized charge in the asymmetric case for different values of colloid radius ( $[\sigma_0] = \text{\AA}$ ) at  $n = 0.001\text{M}$ . Dotted line indicates the PB solution for  $\sigma_0 = 150\text{\AA}$  ( $\kappa\sigma_c \approx 1.6$ ) [16].

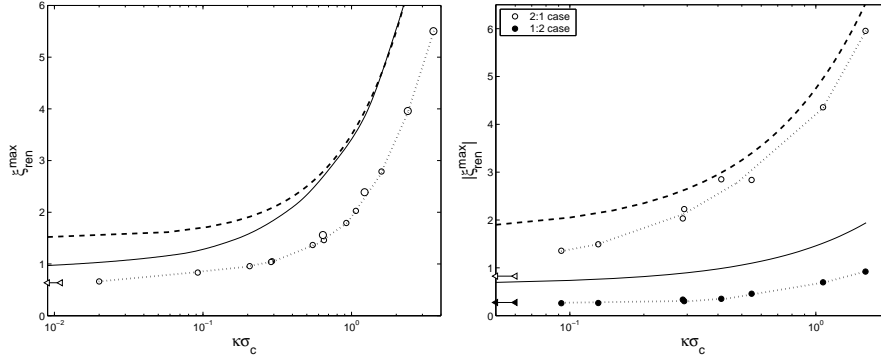


Figure 25: Maximum value of renormalized charge as a function of the reduced radius  $\kappa\sigma_c$  for symmetric (left) and asymmetric (right) electrolyte. At the left, continuous and dashed lines are the theoretical PB upper bound for  $Z_{ren}$  at saturation (analytical prediction from [10] accurate for large  $\sigma$ ) and the PB saturated charge evaluated numerically in [10], respectively. At the right, dashed and continuous lines are, respectively, the PB saturated charges for 2:1 and 1:2 cases [16]. Arrows indicates theoretical PB limit when  $\kappa\sigma_c \rightarrow 0$ . Dotted lines are intended as a guide to eye.